
Electronic band structure of cubic solid-state CdTe_{1-x}Se_x solutions

¹ Ilchuk H. A., ² Andriyevsky B., ³ Kushnir O. S., ^{1*} Kashuba A. I.,
¹ Semkiv I. V. and ¹ Petrus R. Yu.

¹ Department of General Physics, Lviv Polytechnic National University, 12 Bandera Street, 79046 Lviv, Ukraine. * andrii.i.kashuba@lpnu.ua

² Faculty of Electronics and Computer Sciences, Koszalin University of Technology, 2 Sniadeckich Street, 75-453 Koszalin, Poland

³ Electronics and Computer Technologies Department, Ivan Franko National University of Lviv, 107 Tarnavsky Street, 79005 Lviv, Ukraine

Received: 22.02.2021

Abstract. We report on the electronic band structure of solid-state solutions CdTe_{1-x}Se_x (CTS, $0 < x \leq 5/16$) calculated in the framework of density functional theory. The structure of CTS is calculated following from the ‘parent’ binary compound CdTe, which is crystallized in a cubic phase. The bandgap of CTS is found to be of a direct type for all of the solid-state solutions under test. A decrease in the bandgap E_g is found with increasing selenium content x . The $E_g(x)$ dependence reveals some deviations from a simple linear function. The free-carrier concentration increases with increasing selenium content. It is shown that interaction among the atoms of host matrix (CdTe) and substitution selenium atoms causes splitting of the valence bands into heavy-hole and light-hole subbands and spin-orbit splitting, while the conduction bands remain unaffected. The dependence of refractive index on the selenium content is obtained.

Keywords: solid-state solutions, CdTe, concentration dependences, electronic band structure, carrier concentration, refractive index

UDC: 544.225.22, 621.315.592, 535.323

1. Introduction

Cadmium chalcogenides (CdX, with X = S, Se and Te) belong to a A^{II}B^{VI} crystal family and show a typical semiconductor behaviour. They are considered as promising materials for various optoelectronic devices. In particular, CdTe films represent a leading compound for manufacturing cost-effective second-generation (i.e., thin-film-based) photovoltaic devices. CdTe-based solar cells attract much attention of researchers, since CdTe is characterized by a direct forbidden gap and a high optical absorbance (above 10^5 cm^{-1}), which make it an excellent light-absorbing layer for solar cells [1–3].

To form highly efficient p-CdTe-based heterojunctions for the window layers of solar batteries, cadmium sulphide CdS is mainly used, which reveals the bandgap $E_g \sim 2.42 \text{ eV}$ at the room temperature and high optical absorbance [3–6]. This situation has to be considered when searching for any alternatives of CdTe for the solar cells. In particular, ternary solid-state solutions CdTe_{1-x}Se_x (abbreviated hereafter as CTS) can be regarded as a promising semiconductor material. Their additional resource is associated with a dependence of bandgap E_g on selenium content x , which can be used specifically when forming gradient-like structures. It is known that the bandgap energy E_g is equal to 1.44 eV for CdTe [7] and 1.68 eV for CdSe [8, 9]. CdTe has a cubic (zinc-blende) structure [2, 7, 10], whereas CdSe can be materialized in either zinc-blende or hexagonal (wurtzite) structures under normal conditions, depending on the growth conditions [11, 12].

According to the phase diagram [13], the CTS compounds at intermediate x are crystallized in either cubic (at the tellurium contents $x \leq 0.4$) or wurtzite (at $x \geq 0.7$) structures, while the concentration interval $0.4 \leq x \leq 0.7$ corresponds to a break of structural homogeneity.

Some information on the structure and fundamental properties of the CdSe–CdTe system has already been reported in the experimental and theoretical works [13–20]. In particular, crystalline [13, 15, 16, 19] and band [14–19] structures, as well as optical [13, 17–19] and elastic characteristics [15, 16, 20] have been explored. Nonetheless, the properties of these materials still need further investigations. In particular, this concerns the concentration dependences of the bandgap, since the E_g data calculated at some x values are contradictory (see Refs. [16–18]). The dependences of the carrier concentration and the light-hole, heavy-hole and split-off energies on the selenium concentration are also of great interest, especially at relatively small x 's in the solid-state CTS solutions, which correspond to the cubic zinc-blende phase. Note that all the above characteristics are important for optimizing the materials for solar power engineering.

In this report, we study the electronic properties of the solid-state CTS solutions. As an initial crystalline structure of CTS, we have chosen the structure of the ‘pure’ cubic crystals CdTe ($\text{Cd}_{16}\text{Te}_{16}$), in which tellurium atoms are consecutively substituted with selenium ones. Under such conditions, we have performed the band-structure calculations for CTS to obtain the concentration dependences of the bandgap, the carrier concentration, the energy positions of the light-hole and split-off bands, and the refractive index.

2. Calculation details

The band structures of the solid-state CTS solutions ($0 < x \leq 5/16$, with the x -step equal to $\Delta x = 1/16$) were calculated in the framework of a well-known density-functional theory [21], using a CASTEP code [22]. In our calculations, a generalized gradient approximation and a Perdew–Burke–Ernzerhof exchange-and-correlation functional [23] were utilized. Within these techniques, the electronic wave functions were expanded in a plane-wave basic set, using the cut-off energy 310 eV. The electron configurations $4d^{10}5s^2$ for Cd, $5s^25p^4$ for Te and $4s^24p^4$ for Se atoms were taken as the valence ones. A $2 \times 1 \times 2$ supercell containing 32 atoms was created for the density-functional calculations. A $2 \times 4 \times 2$ Monkhorst–Pack mesh was employed for sampling Brillouin zone (BZ) [24]. A self-consistent convergence of the total energy was taken as 5.0×10^{-7} eV/atom. The triclinic symmetry $P\bar{1}$ was kept while optimizing the crystal structure. Geometric optimizations of the lattice parameters and the atomic coordinates were performed using a Broyden–Fletcher–Goldfarb–Shanno minimization technique. The maximal ionic Hellmann–Feynman forces were set within 0.01 eV/Å, the maximum ionic displacement within 5.0×10^{-4} Å, and the maximum stress within 0.02 GPa. These parameters were sufficient to provide a well-converged total energy of the structures.

3. Results and discussion

Earlier, it has been found experimentally [13] that the largest possible selenium content in CTS crystallized in the cubic phase amounts to $x = 0.4$. Therefore we study only the concentrations ranged from 0 to $5/16$, i.e. only the zinc-blende structures. As an example, Fig. 1 presents the band structure calculated for the $\text{Cd}_{16}\text{Te}_{15}\text{Se}$ compound. Here the Fermi level E_F corresponds to the energy $E = 0$. The bandgap of $\text{Cd}_{16}\text{Te}_{15}\text{Se}$ is found to be of direct type, which is denoted as $E_g^{(d)}$ (see Fig. 1). This is typical for all of the CTS compounds under study. In other words, indirect optical transitions that involve phonons can occur in these materials only at the photon energies $h\nu > E_g^{(d)}$. Moreover, this is similar to the situation occurring in the appropriate binary compounds CdTe and CdSe [9, 10].

For all of our crystalline structures, a difference of anisotropies for the valence- and conduction-band dispersions $E(k)$ is evident. The top of the valence band is more flat and the conduction band shows higher dispersion. This is caused by the fact that holes have a less mobility, if compared with electrons. The top of the valence band is mainly formed by p -anionic (Se/Te) and s -cationic (Cd) states, whereas the bottom of the conduction band is formed by p -cationic states. The same is true for pure CdTe [9, 10]. Substitution of tellurium with selenium increases the effective masses of holes and electrons, which can also be seen from the analysis of dispersion $E(k)$ in Fig. 1. This behaviour is evidently caused by the known inverse power-law dependence of the effective mass on the d^2E/dk^2 term. Moreover, the inverse relation between the unit-cell volume V_c and x takes place for the CTS materials. The maximal dispersion $E(k)$ is observed for the bands along the directions G–F and G–Z in the BZ.

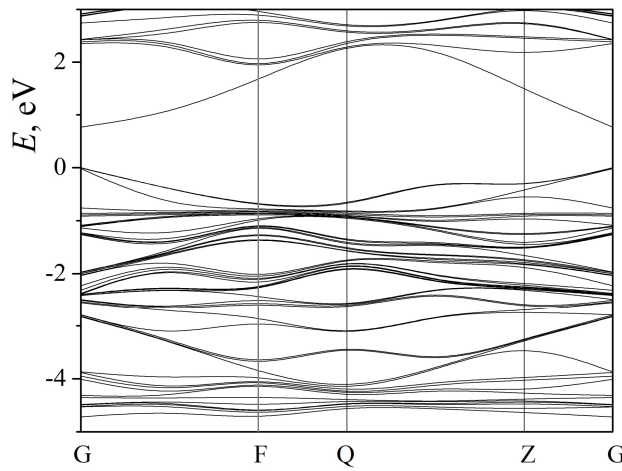


Fig. 1. Electronic band structure for the cubic solid-state $\text{Cd}_{16}\text{Te}_{15}\text{Se}$ solution, as calculated at the points G(0, 0, 0), F(0, 0.5, 0), Q(0, 0.5, 0.5) and Z(0, 0, 0.5) of BZ. The space group is $P1$.

Our analysis of energy-band spectrum for the CTS system testifies that the bandgap E_g is localized in the centre of the BZ, i.e. at the G point. The bandgap E_g for the smallest nonzero concentration $x = 1/16$ (i.e., $\text{Cd}_{16}\text{Te}_{15}\text{Se}$) is calculated as $E_g = 0.770$ eV. Although this value is notably smaller than, e.g., the experimental bandgap known for the pure CdTe compound (1.44 eV [7]), it is well known that the calculations based on the density-functional theory of semiconductors and the local-density or generalized-gradient approximations usually underestimate notably the bandgap [21]. The fundamental optical absorption edge for $\text{Cd}_{16}\text{Te}_{15}\text{Se}$, as well as for all the other compounds under our test, is formed by the direct interband electron transitions. The same is also peculiar for the other binary compounds of cadmium-containing A^{II}B^{VI} materials [9, 10]. Using the experimental data for the bandgap of CdTe [7], we have obtained the value 0.622 eV for a so-called ‘scissor’ factor ΔE (see also Fig. 2). This factor is usually used when comparing the theoretical and experimental optical spectra in the range of electron excitations.

As seen from Fig. 2, the dependence of the bandgap on the selenium content has a decreasing character in the region of relatively small x , which agrees perfectly with the experimental data [13]. Note that the concentration $E_g(x)$ dependence has also been touched upon in the works [16–18]. In particular, the local-density approximation for the cubic CTS has yielded in increasing

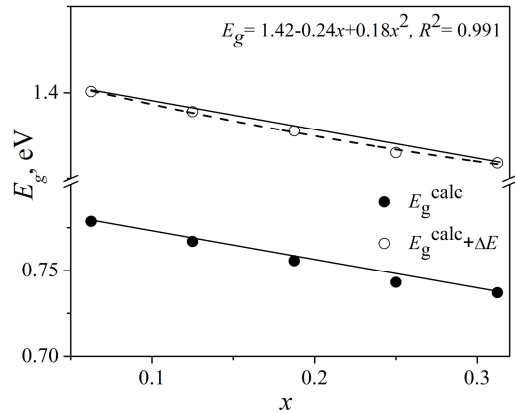


Fig. 2. Concentration dependences $E_g(x)$ of bandgap in the cubic CTS system, as determined directly from *ab initio* calculations (full circles) and using a ‘scissor’ method (open circles). Solid straight lines connect the outermost data points and a dashed line corresponds to quadratic fit explained in the legend.

$E_g(x)$ dependence [16], and the same result has been obtained with the full-potential linearized augmented plane-wave method applied to both the cubic and hexagonal CTS structures [17]. The results derived in Ref. [18] have been less explicit: the full-potential linearized augmented plane-wave method combined with either the generalized gradient approximation or the Engel and Vosko generalized gradient formalism hint at either increasing or decreasing $E_g(x)$ behaviours. Unfortunately, the supercell dimensions used in Refs. [16–18] are unclear, while the corresponding concentration step $\Delta x = 0.25$ is notably larger than ours. Nonetheless, following from our detailed concentration data and the experimental results available for CdTe, CdTe and their solid solutions, we are inclined to suggest that a decreasing $E_g(x)$ dependence should be characteristic for the CTS system at small x (i.e., in the ‘vicinity’ of CdTe compound) and increasing dependence at large x (i.e., in the ‘vicinity’ of CdSe).

As seen from Fig. 2, a straight line, which connects the two limiting selenium concentrations and corresponds to the spirit of a commonly known Vegard’s rule, does not represent the best model when describing the concentration dependence $E_g(x)$ for the CTS system. On the other hand, we obtain a notably higher coefficient of determination, $R^2 = 0.991$, in case of fitting with a quadratic function (see Fig. 2). A principled account of this pattern seems to be a Burstein–Moss effect (see, e.g., Ref. [19, 25]), which is caused by the excess charge carriers (electrons and holes) associated with doping or substituting atoms. To be more specific, the Burstein–Moss effect increases the bandgap in *n*-type semiconductors with a parabolic dispersion law for the energy bands. It arises due to substitution or doping and can be represented in terms of the corresponding bandgap increment ΔE_g (see, e.g., Ref. [25]):

$$\Delta E_g = h^2 (3\pi^2 n_*)^{2/3} / (8\pi^2 m^*), \quad (1)$$

with h being the Planck’s constant, n_* the carrier concentration and m^* the effective electron mass in the conduction band.

One can estimate the concentration of free charge carriers in the CTS solutions, using Eq. (1) and taking the ‘initial’ effective electron mass for CdTe ($m^* = 0.098m_e$ [26], with m_e denoting the free-electron mass). Here the effective mass known for the pure CdTe compound is used, since we have not been able to find in the literature the same parameters for the solid solutions. Fig. 3 testifies that the carrier concentration n_* increases with increasing selenium content x . Here the simplest

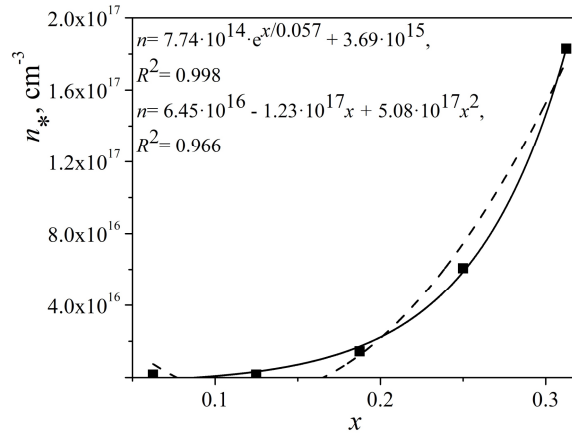


Fig. 3. Dependence of free-carrier concentration n_* on tellurium content x for the cubic CTS system, as obtained using Eq. (1). Solid and dashed lines correspond to exponential and quadratic fits (see the legend).

quadratic function employed earlier to describe the behaviour of the bandgap does not represent the best fitting of the concentration dependence $n_*(x)$ for the CTS system ($R^2 \approx 0.966$). However, we obtain a very high R^2 value (0.998) when fitting the data with a single-exponential function. A possible meaning of this fact has to be explored in further studies.

It is a well-known fact that interaction among the atoms of host matrix (CdTe in our case) and substituting atoms (i.e., selenium) should split the energy bands into heavy-hole and light-hole bands and spin-orbit splitting of the valence bands, while the conduction bands remains unaffected. This situation has earlier been found, e.g., in a ternary $\text{GaSb}_{1-x}\text{Bi}_x$ system [27] (see also the physical argumentation quoted in Ref. [27]). The concentration dependences for the electronic bands mentioned above are shown in Fig. 4. It is evident that their positions are shifted towards higher energies with increasing selenium concentration. Moreover, the concentration dependences are nearly linear ($R^2 \sim 0.91 \div 0.95$), with no simple alternative fitting function available. Note also that the heavy-hole band energy is in fact invariable in the scale of Fig. 4 and corresponds to a zero level.

Now we proceed to the refractive index, which represents a fundamental optical parameter related to the band structure of optoelectronic materials. A number of empirical relationships linking the refractive index n with the bandgap E_g are known from the literature, the most

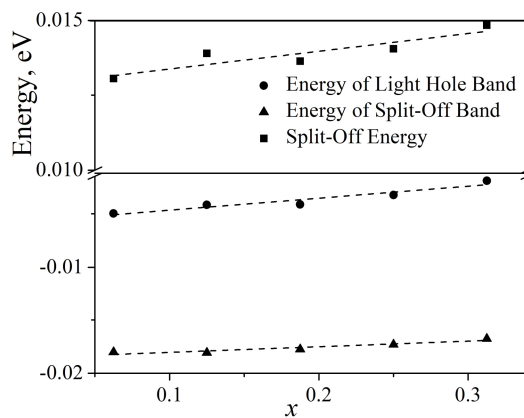


Fig. 4. Concentration dependences of the energy positions of different bands (see the legend), as calculated for the cubic CTS system at the G point of BZ. Lines correspond to linear fits.

notorious of which are those suggested by Moss [28], Ravindra [29], Herve and Vandamme [30], and Tripathy [31]. According to these models, a refractive index of a semiconductor (with a bandgap being usually inside the range $0 < E_g < 5$ eV) can be found as

$$n_M^4 E_g = C, \quad n_R = a - bE_g, \quad n_{H-V}^2 = 1 + [A/(E_g + B)]^2, \quad n_T = n_0[1 + \alpha e^{-\beta E_g}]. \quad (2)$$

Here the subscripts “M”, “R”, “H–V” and “T” imply that the refractive index is calculated using the Moss, Ravindra, Herve–Vandamme and Tripathy relations, respectively. In Eqs. (2), the normal conditions are assumed, the bandgap units are eV, and the n ’s subscripts abbreviate the authors mentioned above. In Eqs. (2), We have $C = 95$ eV, $a = 4.084$ eV, $b = 0.62$ eV⁻¹, $A = 13.6$ eV, $B = 3.47$ eV, $n_0 = 1.73$, $\alpha = 1.9017$ and $\beta = 0.539$ eV⁻¹ [28–31]. In spite of a wide variety of empirical relationships, sometimes there arise some problems with interpreting quantitatively the refractive index in terms of Eqs. (2) and preferring one formula over the other (see Refs. [32–34]).

Using different models given by Eqs. (2), we have calculated the n values for the cubic CTS system, which correspond to the photon energies $h\nu$ exactly equal to the bandgaps. Note that the calculated bandgaps E_g used by us include the ‘scissor’ factor, while our n ’s are not iso-frequency. Fig. 5 displays the appropriate theoretical dependences $n(x)$ on the selenium concentration. Here the Tripathy and Moss formulae predict respectively the largest and the smallest refractive index values.

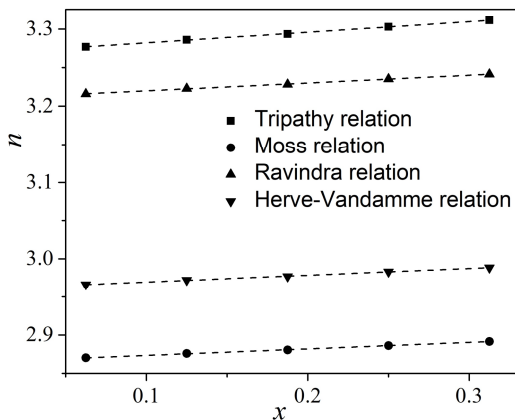


Fig. 5. Concentration dependences of refractive index for the cubic CTS system, as calculated according to different theoretical models (see the legend). Lines correspond to linear fits with the coefficients of determination > 0.99 .

Unfortunately, we could not find in the literature the experimental results for the refractive indices of CTS at any intermediate selenium concentration. Nonetheless, one can still make an experiment–theory comparison when taking the experimental data for pure CdTe ($n = 2.865$ at the wavelength 861 nm [3]) and balancing it against the calculated data of Fig. 5 extrapolated to the concentration $x = 0$. It turns out that the refractive index obtained with the Moss formula is only $< 0.01\%$ different from the experimental one. The relative accuracy of the Herve–Vandamme formula remains high enough (3.3%), whereas the Ravindra and Tripathy formulae provide somewhat poorer results (11.4% and 13.1%, respectively). As a conclusion, the canonical Moss relationship between the refractive index and the bandgap works extremely well in case of the cubic CTS system and can be employed to predict the optical properties of the compounds with any x in the interval $0 < x \leq 5/16$.

Conclusion

Summing up, we have studied theoretically the electronic band structure for the solid-state CTS solutions described by the cubic structure. The selenium-content range $x = 0 \div 5/16$ has been covered. It has been shown that the bandgap decreases with increasing selenium concentration in the CTS system. The smallest bandgap is of the direct type for all the compounds under study. The concentration dependence of the bandgap energy can be satisfactorily described by a quadratic function. This behaviour is presumably explained by the Burstein–Moss effect.

The concentration n_* of free charge carriers in the cubic CTS system has the order of magnitude $\sim 10^{17} \text{ cm}^{-3}$ at the maximal selenium concentration $x = 5/16$. The increase in this concentration occurring with increasing selenium content can be formally described by a single-exponential function. The parameters associated with the light-hole and split-off energies increase with increasing selenium concentration. This behaviour should imply increasing mobility of free carriers and so increasing electrical conductivity. Finally, the refractive index calculated from the bandgap and the Moss formula agrees very well with the available experimental data.

Following from the results obtained in the present work, we suppose that the solid-state cubic CTS system can prove a promising material for the solar cells and, in particular, the heterojunction structures built on thin films.

Acknowledgements

The work is supported by the Project #0119U002247 of Ministry of Education and Science of Ukraine. Computer simulations are performed using the CASTEP code at the ICM of the Warsaw University (the Project #G81-13) and at the WCSS of the Wrocław University of Technology (the Project #053).

References

1. Romeo N, Bosio A, Tedeschi R and Canevari V, 2000. Growth of polycrystalline CdS and CdTe thin layers for high efficiency thin film solar cells. *Mater. Chem. Phys.* **66**: 201–206.
2. McCandless B E and Dobson K D, 2004. Processing options for CdTe thin film solar cells. *Sol. Energy.* **77**: 839–856.
3. Treharne R E, Seymour-Pierce A, Durose K, Hutchings K, Roncallo S and Lane D, 2011. Optical design and fabrication of fully sputtered CdTe/CdS solar cells. *J. Phys.: Conf. Ser.* **286**: 012038.
4. Basola B M and McCandless B, 2014. Brief review of cadmium telluride-based photovoltaic technologies. *J. Photon. Energy.* **4**: 040996.
5. Romeo N, Bosio A, Canevari V and Podesta A, 2014. Recent progress on CdTe/CdS thin film solar cells. *Sol. Energy.* **77**: 795–801.
6. Paudel N R, Xiao C and Yan Y, 2014. Close-space sublimation grown CdS window layers for CdS/CdTe thin-film solar cells. *J. Mater. Sci.: Mater. Electron.* **25**: 1991–1998.
7. Petrus R, Ilchuk H, Kashuba A, Semkiv I and Zmiiovska E, 2020. Optical properties of CdTe thin films obtained by the method of high-frequency magnetron sputtering. *Funct. Mater.* **27**: 342–347.
8. Ilchuk H, Petrus R, Kashuba A, Semkiv I and Zmiiovska E, 2020. Optical-energy properties of CdSe thin film. *Mol. Cryst. Liq. Cryst.* **699**: 1–8.
9. Il'chuk G A, Petrus R Yu, Kashuba A I, Semkiv I V and Zmiiovs'ka E O, 2020. Peculiarities of the optical and energy properties of thin CdSe films. *Opt. Spectrosc.* **128**: 50–57.
10. Ilchuk H A, Petrus R Yu, Kashuba A I, Semkiv I V and Zmiiovska E O, 2018. Optical-energy properties of the bulk and thin-film cadmium telluride (CdTe). *Nanosystems, Nanomaterials, Nanotechnologies.* **16**: 519–533.

11. Kale R B and Lokhande C D, 2005. Band gap shift, structural characterization and phase transformation of CdSe thin films from nanocrystalline cubic to nanorod hexagonal on air annealing. *Semicond. Sci. Technol.* **20**: 1.
12. Kainthla R C, Pandya D K and Chopra K L, 1980. Solution growth of CdSe and PbSe films. *J. Electrochem. Soc.* **127**: 277.
13. Poplawsky J D, Guo W, Paudel N, Ng A, More K, Leonard D and Yan Y, 2016. Structural and compositional dependence of the $\text{CdTe}_x\text{Se}_{1-x}$ alloy layer photoactivity in CdTe-based solar cells. *Nature Commun.* **7**: 12537.
14. Reshak A H and Jamal M, 2017. Investigation of pressure-induced phase transitions of the solar cell materials $\text{CdTe}_x\text{Se}_{1-x}$ alloys: one- and two-dimensional search DFT calculation. *Phase Trans.* **90**: 1155–1166.
15. Jamal M, Abu-Jafar M S and Dahliah D, 2017. Disclosing the structural, phase transition, elastic and thermodynamic properties of $\text{CdTe}_x\text{Se}_{1-x}$ ($x = 0.0, 0.25, 0.5, 0.75, 1.0$) using LDA exchange correlation. *Results in Physics*. **7**: 2213–2223.
16. Shakil M, Zafar M, Ahmed S, Hashmi R M, Choudhary M A and Iqbal T, 2016. Theoretical calculations of structural, electronic, and elastic properties of $\text{CdTe}_x\text{Se}_{1-x}$: A first principles study. *Chin. Phys. B*. **25**: 076104.
17. Reshak A H, Kityk I V, Khenata R and Auluck S, 2011. Effect of increasing tellurium content on the electronic and optical properties of cadmium selenide telluride alloys $\text{CdTe}_x\text{Se}_{1-x}$: An *ab initio* study. *J. Alloys and Comp.* **509**: 6737–6750.
18. Ouendadji S, Ghemid S, Bouarissa N, Meradji H and El Haj Hassan F, 2011. *Ab initio* study of structural, electronic, phase diagram, and optical properties of $\text{CdTe}_x\text{Se}_{1-x}$ semiconducting alloys. *J. Mater. Sci.* **46**: 3855–3861.
19. Kashuba A I, Ilchuk H A, Petrus R Yu, Andriyevsky B, Semkiv I V and Zmiyovska E O, 2021. Growth, crystal structure and theoretical studies of energy and optical properties of $\text{CdTe}_x\text{Se}_{1-x}$ thin films. *Appl. Nanosci.*
20. Ilchuk H A, Korbutyak D V, Kashuba A I, Andriyevsky B, Kupchak I M, Petrus R Yu and Semkiv I V, 2020. Elastic properties of $\text{CdTe}_x\text{Se}_{1-x}$ ($x = 1/16$) solid solution: first principles study. *Semicond. Phys., Quant. Electron. & Optoelectron.* **23**: 355–360.
21. Andriyevsky B, Kashuba A I, Kunyo I M, Dorywalski K, Semkiv I V, Karpa I V, Stakhura V B, Andriyevska L, Piekarski J and Piasecki M, 2019. Electronic bands and dielectric functions of $\text{In}_{0.5}\text{Tl}_{0.5}\text{I}$ solid state solution with structural defects. *J. Electron. Mater.* **48**: 5586–5594.
22. Clark S J, Segall M D, Pickard C J, Hasnip P J, Probert M J, Refson K and Payne M C, 2005. First principles methods using CASTEP. *Z. Kristallogr.* **220**: 567–570.
23. Perdew J P, Ruzsinszky A, Csonka G I, Vydrov O A, Scuseria G E, Constantin L A, Zhou X and Burke K, 2008. Restoring the density-gradient expansion for exchange in solids and surfaces. *Phys. Rev. Lett.* **100**: 136406.
24. Monkhorst H J and Pack J D, 1976. Special points for Brillouin-zone integrations. *Phys. Rev. B*. **13**: 5188.
25. Turko B, Mostovoy U, Kovalenko M, Eliyashevskyi Y, Kulyk Y, Bovgyra O, Dzikovskyi V, Kostruba A, Vlokh R, Savaryn V, Stybel V, Tsizh B and Majevska S, 2021. Effect of dopant concentration and crystalline structure on the absorption edge in $\text{ZnO}:Y$ films. *Ukr. J. Phys. Opt.* **22**: 31–37.
26. Freik D M, Chobanyuk V M, Krutnitsky O S and Gorichok I V, 2012. Photovoltaic solar energy converters based on cadmium telluride II. The main achievements and current status (Review). *Phys. Chem. Solid State*. **13**: 744–758.

27. Das S, Bhowal M K and Dhar S, 2019. Calculation of the band structure, carrier effective mass, and the optical absorption properties of GaSbBi alloys. *J. Appl. Phys.* **125**: 075705.
28. Moss T A, 1950. Relationship between the refractive index and the infra-red threshold of sensitivity for photoconductors. *Proc. Phys. Soc. B.* **63**: 167–176.
29. Ravindra N M, Auluck S and Srivastava V K, 1979. On the Penn gap in semiconductors. *Phys. Stat. Solidi (b)*. **93**: K155–K160.
30. Herve P J L and Vandamme L K J, 1995. Empirical temperature dependence of the refractive index of semiconductors. *J. Appl. Phys.* **77**: 5476–5477.
31. Tripathy S K, 2015. Refractive indices of semiconductors from energy gaps. *Opt. Mater.* **46**: 240–246.
32. Anani M, Mathieu C, Lebid S, Amar Y, Chama Z and Abid H, 2008. Model for calculating the refractive index of a III–V semiconductor. *Comput. Mat. Sci.* **41**: 570–575.
33. Reddy R R, Ram Gopal K, Narasimhulu K, Reddy L S S, Kumar K R, Balakrishnan G and Ravi Kumar M, 2009. Interrelationship between structural, optical, electronic and elastic properties of materials. *J. Alloys Comp.* **473**: 28–35.
34. Kushnir O S, Shchepanskyi P A, Stadnyk V Yo and Fedorchuk A O, 2019. Relationships among optical and structural characteristics of ABSO_4 crystals. *Opt. Mater.* **95**: 109221.

Ilchuk H. A., Andriyevsky B., Kushnir O. S., Kashuba A. I., Semkiv I. V. and Petrus R. Yu. 2021. Electronic band structure of cubic solid-state $\text{CdTe}_{1-x}\text{Se}_x$ solutions. *Ukr.J.Phys.Opt.* **22**: 101 – 109. doi: 10.3116/16091833/22/2/101/2021

Анотація. У рамках теорії функціонала густини розраховано електронну зонну структуру твердотільних розчинів $\text{CdTe}_{1-x}\text{Se}_x$ (CTS , $0 < x \leq 5/16$). Структуру CTS одержано, виходячи з «материнської» бінарної сполуки CdTe , яка кристалізується в кубічній фазі. Встановлено, що всі вивчені нами твердотільні розчини CTS є прямозонними. Виявлено звуження ширини щілини E_g зі зростанням вмісту селену x . Залежність $E_g(x)$ деяко відхиляється від лінійної. Концентрація вільних носіїв зростає зі зростанням вмісту селену. Показано, що взаємодія між атомами матриці-господаря (CdTe) та атомами заміщення селену викликає розщеплення валентних смуг на важкі діркові та легкі діркові підзони, а також спін-орбітальне розщеплення, тоді як смуги провідності залишаються незмінними. Одержано залежність показника заломлення від вмісту селену.